

# Photoelectrochemically Fabricated and Heated Cu<sub>2</sub>O/CuO Bilayers with Enhanced Photovoltaic Characteristics

Masanobu Izaki,\* Suzuka Abe, Kota Nakakita, and Pei Loon Khoo

Cite This: *ACS Omega* 2021, 6, 27587–27597

Read Online

ACCESS |



Metrics &amp; More

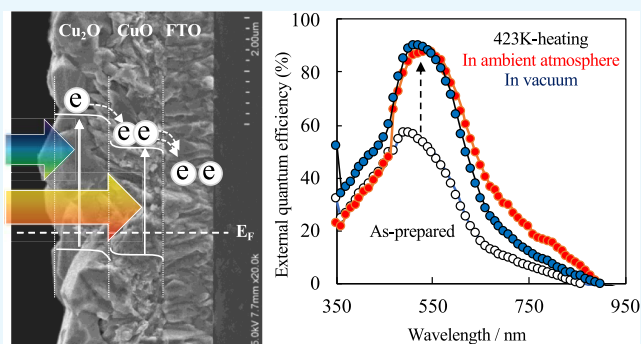


Article Recommendations



Supporting Information

**ABSTRACT:** Cu<sub>2</sub>O/CuO bilayers were fabricated by electro-deposition of the CuO layer in a copper(II)–ammonia complex aqueous solution, followed by photoelectrochemical deposition of the Cu<sub>2</sub>O layer at potentials ranging from  $-0.3$  to  $-1.0$  V referenced to a Ag/AgCl electrode in a copper(II)–lactate complex aqueous solution under light irradiation, and the effects of varied potentials of the photoelectrochemical Cu<sub>2</sub>O depositions and post-heating conditions on their structural, optical, and photovoltaic characteristics were investigated with X-ray diffraction, field emission-scanning electron microscopy, optical absorption measurements, and external quantum efficiency (EQE) measurements with and without applied bias voltage. The Cu<sub>2</sub>O layers with a characteristic 2.1 eV band gap energy were adhesively stacked on the thorn-like grains of the CuO layers possessing a characteristic 1.5 eV band gap energy, and dense and defect-free Cu<sub>2</sub>O/CuO bilayers could be fabricated at the potentials of  $-0.4$  and  $-0.5$  V, but the grain size of Cu<sub>2</sub>O decreased at  $-0.5$  V. In addition, the metallic Cu was deposited simultaneously at potentials less than  $-0.7$  V. The Cu<sub>2</sub>O/CuO bilayer fabricated at  $-0.4$  V revealed photovoltaic features at wavelengths ranging from 350 nm to approximately 900 nm, and a maximum EQE value of 56.8% was achieved at 510 nm in wavelength with a bias voltage of  $-0.1$  V. The maximum EQE value, however, decreased to 1.2% accompanied with the peak wavelength shift to 580 nm, and no photovoltaic feature was observed at potentials of  $-0.3$ ,  $-0.7$ , and  $-1.0$  V. The photovoltaic performance for the Cu<sub>2</sub>O/CuO bilayer fabricated at  $-0.4$  V was ameliorated by heating at 423 K, and the maximum EQE values were enhanced to 87.7% at 550 nm and 89.8% at 530 nm in an ambient atmosphere and vacuum. Both the Cu<sub>2</sub>O and CuO layers acted as photovoltaic layers in the Cu<sub>2</sub>O/CuO bilayer fabricated at  $-0.4$  V and heated at 423 K, and the electrical characteristic including the carrier mobility affected the photovoltaic performance. The photovoltaic feature, however, disappeared by heating above 523 K due to the formation of nanopores inside the CuO layer and near the CuO heterointerface to the Cu<sub>2</sub>O and fluorine-doped tin oxide substrate.



## INTRODUCTION

Harvesting solar energy as a sustainable source of energy has always been a growing field of interest, with increased focus in the research of p-type semiconductors that can convert solar irradiation into electricity in solar cells<sup>1,2</sup> and into chemical energy in the form of hydrogen gas by photoelectrochemically water-splitting in photocathodes.<sup>3</sup> The photovoltaic conversion process is composed of three steps: excitation of electrons from the valence band to conduction band by light absorption when irradiated by photon energies larger than the band gap energy of the photoactive layer, resulting in the formation of excitons consisting of electron–hole pairs; dissociation of the excitons to free carriers; and the transportation of carriers by the electric field formed at the heterointerface.<sup>4,5</sup> Thus, the conversion efficiency for single p–n-heterojunction solar cells is closely related to the band gap energy of the p-semiconductor, and the theoretical conversion efficiency is predicted to be approximately 28% under the irradiation of AM1.5 illumination (1 sun).<sup>6</sup>

To further enhance conversion efficiency, the expansion of the light-absorption band and enhancement of the quantum efficiency are necessary, and introducing two or more p-type semiconductors with different band gap energies in a light-absorbing layer is a promising strategy to overcome the limitation of band gap energy-originated theoretical conversion efficiency imposed on single solar cells,<sup>7</sup> as demonstrated by a InGaP/GaAs/InGaAs triple-junction tandem solar cell with a 33.7% conversion efficiency.<sup>8</sup>

Copper oxides of Cu<sub>2</sub>O<sup>9</sup> and CuO<sup>10</sup> are p-type semiconductors with the band gap energies of 2.1 and 1.4 eV, and

Received: September 17, 2021

Accepted: September 30, 2021

Published: October 8, 2021



both have been applied as photovoltaic layers in oxide solar cells,<sup>11–13</sup> and as photocathodes to generate hydrogen gas by photoelectrochemical water splitting.<sup>14–16</sup> Also, p-Cu<sub>2</sub>O/p-CuO bilayers have attracted increasing attention as photoactive layers which satisfy the aforementioned multi-band gap strategy to enhance the performance.<sup>17–19</sup> The Cu<sub>2</sub>O and CuO layers had been prepared by several techniques of thermal oxidation of metallic Cu,<sup>20,21</sup> gas-phase deposition processes such as sputtering and pulsed laser deposition,<sup>22,23</sup> and solution chemical processes which include electrochemical processes.<sup>24–26</sup> The Cu<sub>2</sub>O/CuO bilayers have been prepared by several ways composed of chemical preparations followed by heating,<sup>27,28</sup> and the improved photovoltaic and photocathode characteristics have been demonstrated for those prepared by the Cu<sub>2</sub>O electrodeposition followed by subsequent thermal oxidation in air.<sup>17,18</sup> The Cu<sub>2</sub>O/CuO bilayers showed a widened photovoltaic wavelength range originating from both the Cu<sub>2</sub>O and CuO layers, but the external quantum efficiency (EQE) was low, compared to those for the single Cu<sub>2</sub>O and CuO layers.<sup>29,30</sup> The introduction of nanopores into the Cu<sub>2</sub>O layer and structural change in the grains of the CuO layer were brought forth by heating, which pose detrimental effects on the photovoltaic characteristic.<sup>17</sup> In the case of electrochemical fabrication of a Cu<sub>2</sub>O/CuO bilayer in a copper(II)–lactate complex aqueous solution, the challenge lies not in the initial electrodeposition of Cu<sub>2</sub>O layer but in the subsequent electrodeposition of the CuO layer, which needs electrons, which are the minority carriers in the underlying Cu<sub>2</sub>O layer. We have demonstrated a method of direct fabrication of the Cu<sub>2</sub>O/CuO and CuO/Cu<sub>2</sub>O bilayers by photoelectrochemical reactions in which the electrons as minority carriers were increased by light irradiation of photon energies larger than the band gap energy of CuO.<sup>31</sup>

Here, we report the fabrication of Cu<sub>2</sub>O/CuO bilayers by first electrodepositing CuO in a copper(II)–ammonia complex aqueous solution, followed by a photoelectrochemical deposition of the Cu<sub>2</sub>O layer in a copper(II)–lactate complex aqueous solution under light irradiation, and the effects of the potentials of the Cu<sub>2</sub>O photoelectrochemical depositions and post-heating conditions on the structural, optical, and photovoltaic characteristics were investigated by X-ray diffraction, field emission scanning electron microscopy (FE-SEM) observation, optical absorption spectra measurements, and EQE measurements with and without bias voltage, in addition to the electrochemical measurements for the photoelectrochemical Cu<sub>2</sub>O depositions. A dense and defect-free Cu<sub>2</sub>O/CuO bilayer had been fabricated at  $-0.4$  V (vs Ag/AgCl), and the bilayer revealed a maximum EQE of 56.8% under an applying a bias voltage of  $-0.1$  V. The EQE maximum value was further enhanced to 89.8 and 87.7% by heating at 423 K in an ambient atmosphere and vacuum, but its photovoltaic feature disappeared when heated over 523 K due to the formation of nanopores.

## EXPERIMENTAL SECTION

The Cu<sub>2</sub>O/CuO bilayers were fabricated on a F:SnO<sub>2</sub>/SLG (FTO) substrate (AGC Fabritec, Co. Ltd.) by electrodeposition of the CuO layer followed by the photoelectrochemical deposition of the Cu<sub>2</sub>O layer. The CuO layer was prepared by anodic deposition at a potential of 0.85 V referenced to the Ag/AgCl electrode for 1 C/cm<sup>2</sup> at 298 K in an aqueous solution containing 0.05 mol/L copper(II)

nitrate hydrate, 0.05 mol/L ammonium nitrate, and 3.3 mL/L ammonia water (28–30%) with a Potentio/Galvanostat (Hokuto Denko, HA-151A) connected with a Coulomb meter (Hokuto Denko, HF-201). Cu<sub>2</sub>O layers were stacked on the CuO layers by cathodic depositions at potentials  $-0.3$  to  $-1.0$  V (vs Ag/AgCl) for 1 C/cm<sup>2</sup> at 313 K in an aqueous solution containing 0.4 mol/L copper(II)acetate hydrate and 3 mol/L lactic acid at pH 12.5 under a light irradiation with an automatic polarization system (Hokuto Denko, HSV-100) connected to a Coulombmeter (Hokuto Denko, HF-201). Light was irradiated from the side of the glass substrate using a high-pressure mercury lamp (USHIO, OPTICAL-MODULEX, 500 W). The solutions were prepared with reagent-grade chemicals, and distilled water was purified by Millipore Ellix-UV-Advantage. Prior to the fabrications, the FTO substrates were degreased by anodic polarizations at 0.1 mA cm<sup>-2</sup> for 1 min in a 1 mol/L NaOH aqueous solution. Heating in an ambient atmosphere and vacuum was performed at temperatures of 423, 473, 523, and 573 K for 1 h using a rapid thermal annealing system with an infrared lamp (ULVAC-KIKO, MILA-5000) connected to an oil diffusion vacuum pump system ( $\sim 10^{-3}$  Pa, ULVAC-KIKO, VPC-051).

X-ray diffraction measurements were performed using Rigaku RINT2500 with a  $\theta/2\theta$  scanning technique using Cu K $\alpha$  radiation. The surface and cross-sectional structures were observed with a FE-SEM (Hitachi High-Technology, SU-8000). The optical absorption spectra were recorded with a UV–vis–NIR spectrophotometer (Hitachi High-Technology, U4100) referenced to the bare FTO substrate. The EQE was measured at wavelengths ranging from 300 to 1200 nm with and without bias voltages ranging from 0 to  $-0.1$  V using a spectral response measurements system (Bunko Keiki, SM250KB). For the EQE measurements of the devices, Au electrodes on the Cu<sub>2</sub>O layer and In electrodes on the FTO bare layer were prepared with a physical vapor deposition system in vacuum (ULVAC-KIKO, VPC260F).

## RESULTS AND DISCUSSION

**Photoelectrochemically Fabricated Cu<sub>2</sub>O/CuO Bilayers and the Photovoltaic Characteristics.** Figure 1 shows the linear sweeping voltammograms for the Cu<sub>2</sub>O electrodepositions on the CuO layer with and without light irradiation. In the absence of light irradiation, current density

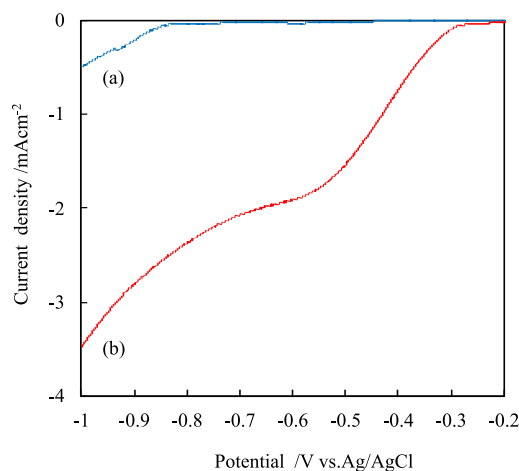
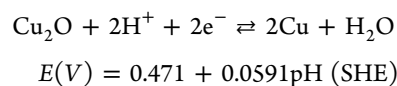
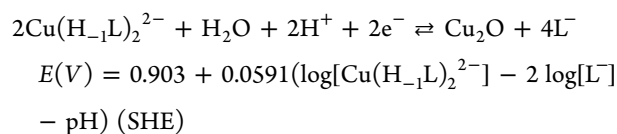


**Figure 1.** Potential–current density curves for the Cu<sub>2</sub>O electrodeposition in dark (a) and under light irradiation (b).

was limited to a low level below  $-0.03 \mu\text{A cm}^{-2}$  at potentials more positive than  $-0.8 \text{ V}$ , which increased gradually to  $-0.5 \text{ mA cm}^{-2}$  at  $-1.0 \text{ V}$ . No evidence of  $\text{Cu}_2\text{O}$  electrodeposition could be observed irrespective of the deposition potentials without light irradiation. As seen here, light irradiation induced a drastic increase in current density at potentials more negative than  $-0.28 \text{ V}$ . When the potential was decreased below  $-0.5 \text{ V}$ , the current density had increased to  $-1.54 \text{ mA cm}^{-2}$ , which was approximately 100 times compared to that without light irradiation. The current density increased further after a small plateau at around  $-0.58 \text{ V}$  and reached  $-3.47 \text{ mA cm}^{-2}$  at  $-1.0 \text{ V}$ . Because lights with photon energies larger than the band gap energy of the  $\text{CuO}$  layer constituted a considerably large portion of the light spectrum emitted by the high-pressure mercury lamp, such lights induced the absorption of energy and consequently caused excitation of electrons from the valence to conduction band in the  $\text{CuO}$  layer, which were then swept toward the solution by the electric field formed at the heterointerface between the  $\text{CuO}$  layer and solution, which facilitated the  $\text{Cu}_2\text{O}$  electrodeposition. The increase in current density originated from the increase in minority carrier of electrons needed for the  $\text{Cu}_2\text{O}$  electrodeposition by light irradiation. According to the solution and electrochemical analyses for the  $\text{Cu}$ -lactate complex solution, the dissolved species exists as  $\text{Cu}(\text{H}_{-1}\text{L})_2^{2-}(\text{aq})$  at  $\text{pH } 12.5$ , and the reduction reactions and equilibrium potentials for the  $\text{Cu}(\text{H}_{-1}\text{L})_2^{2-}/\text{Cu}_2\text{O}$  and  $\text{Cu}_2\text{O}/\text{Cu}$  reactions can be described as follows<sup>32,33</sup>



The equilibrium potentials for the  $\text{Cu}(\text{H}_{-1}\text{L})_2^{2-}/\text{Cu}_2\text{O}$  and  $\text{Cu}_2\text{O}/\text{Cu}$  reactions were roughly calculated to be  $-0.18$  and  $-0.47 \text{ V}$  referenced to an  $\text{Ag}/\text{AgCl}$  electrode at  $\text{pH } 12.5$  by assuming  $[\text{Cu}(\text{H}_{-1}\text{L})_2^{2-}] = 0.4$ , and  $[\text{L}^-] = 3$ . The potentials at which the current density began to increase in the negative direction were roughly estimated to be  $-0.28$ , and  $-0.58 \text{ V}$ , respectively, on the linear sweeping voltammogram with light irradiation, and these potentials were more negative than those calculated for the reactions of  $\text{Cu}(\text{H}_{-1}\text{L})_2^{2-}/\text{Cu}_2\text{O}$  and  $\text{Cu}_2\text{O}/\text{Cu}$ . The first and second increases in current density were attributed to the electrodeposition of  $\text{Cu}_2\text{O}$  and metallic  $\text{Cu}$ , suggesting a co-deposition of metallic  $\text{Cu}$  and  $\text{Cu}_2\text{O}$  at potentials more negative than  $-0.58 \text{ V}$ .

Figure 2 shows the X-ray diffraction patterns for  $\text{Cu}_2\text{O}/\text{CuO}$  bilayers prepared at potentials ranging from  $-0.3$  to  $-1.0 \text{ V}$  for the  $\text{Cu}_2\text{O}$  depositions. All diffracted X-ray peaks can be identified as those for  $\text{Cu}_2\text{O}$  (cuprite) with a characteristic cubic lattice,<sup>34</sup> and  $\text{CuO}$  (tenorite) with a characteristic monoclinic lattice<sup>35</sup> for all the  $\text{Cu}_2\text{O}/\text{CuO}$  bilayers irrespective of the potentials, excluding the peaks which originated from  $\text{SnO}_2$  of the FTO substrate. In addition,  $\text{Cu}(111)$  peaks can be observed at  $43.56^\circ$  for the  $\text{Cu}_2\text{O}/\text{CuO}$  bilayers prepared at  $-0.7$  and  $-1.0 \text{ V}$ , which deposition potentials were more negative than equilibrium potential of the  $\text{Cu}_2\text{O}/\text{Cu}$  reaction. From here, it can be confirmed that electrodepositions of  $\text{Cu}_2\text{O}$  occurred on the  $\text{CuO}$  layer under light irradiation, while

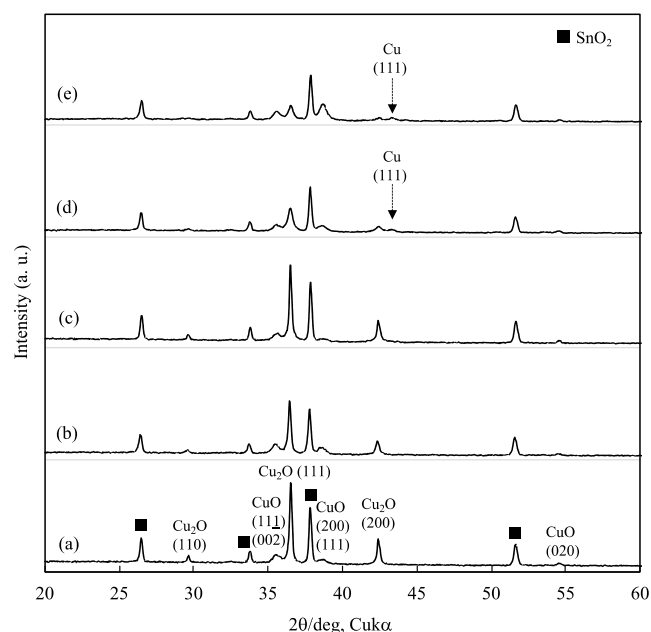


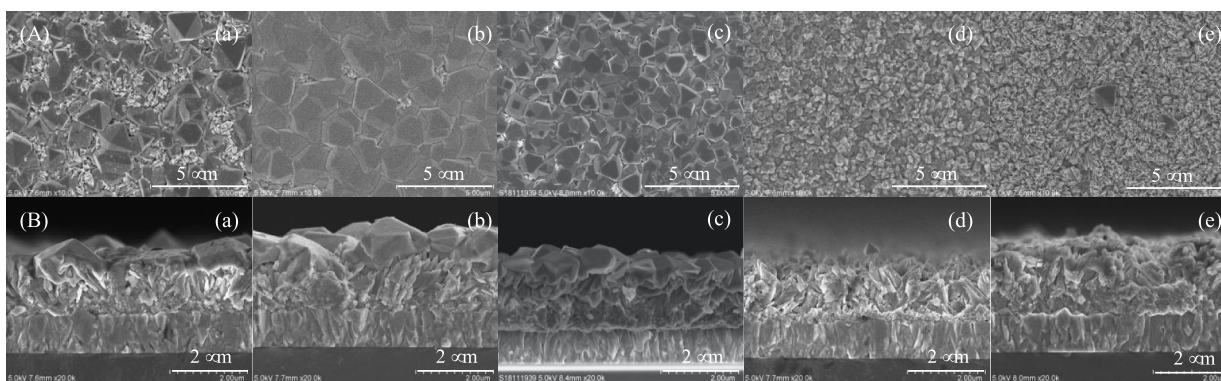
**Figure 2.** X-ray diffraction patterns for  $\text{Cu}_2\text{O}/\text{CuO}$  bi-layers prepared at  $-0.3$  (a),  $-0.4$  (b),  $-0.5$  (c),  $-0.7$  (d), and  $-1.0 \text{ V}$  (e) for the photoelectrochemical  $\text{Cu}_2\text{O}$  deposition.

there were no deposits without light irradiation. The electrodepositions of  $\text{Cu}_2\text{O}$  showed no effects on the profiles of diffracted X-ray peaks identified as  $\text{CuO}$ , including its peak angle, full width at half maximum (fwhm), and intensity ratios.

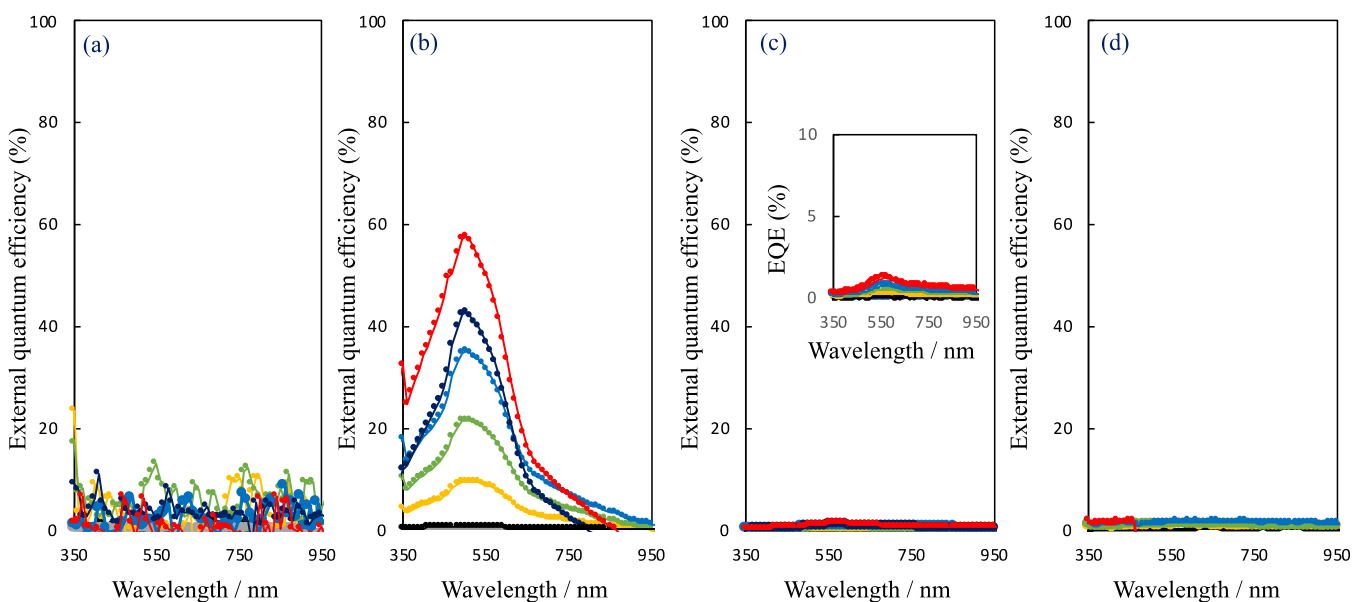
Peak angles of the  $\text{Cu}_2\text{O}$  (110), (111), and (200) planes were almost constant irrespective of the potentials, and the lattice constant calculated from the peak angles was estimated to be  $0.2641 \text{ nm}$ , which is close to the reported standard value.<sup>34</sup> The effect of the potential on the fwhm value of the  $\text{Cu}_2\text{O}$  (111) peak is shown in Figure S1. The fwhm values were almost constant around  $0.23^\circ$  at potentials ranging from  $-0.3$  to  $-0.5 \text{ V}$  and increased to more than  $0.40^\circ$  at potentials below  $-0.7 \text{ V}$ . Because the intensity ratios for the  $\text{Cu}_2\text{O}$  (110), (111), and (200) peaks were almost constant irrespective of the potentials, the  $\text{Cu}_2\text{O}$  layers possessed a similar preferred orientation. The distinct preferred orientation of the  $\text{Cu}_2\text{O}$  layers and effects of the orientation of the under  $\text{CuO}$  layer were not clear at present. The intensity of the  $\text{Cu}_2\text{O}$  peaks decreased at potentials below  $-0.7 \text{ V}$  due to the reduction of the total amount of the  $\text{Cu}_2\text{O}$  due to consumption of electric charge by the reduction reaction to metallic  $\text{Cu}$ .

Figure 3 shows surface and cross-sectional images for  $\text{Cu}_2\text{O}/\text{CuO}$  bilayers prepared at  $-0.3$  to  $-1.0 \text{ V}$  for the  $\text{Cu}_2\text{O}$  depositions. The  $\text{CuO}$  layer was composed of aggregates of thorn-like grains grown from the FTO substrate. Angular  $\text{Cu}_2\text{O}$  grains with approximately  $454 \text{ nm}$  in size were adhesively deposited on the  $\text{CuO}$  layer at  $-0.3 \text{ V}$ , and exposed thorn-like  $\text{CuO}$  grains were observed between the  $\text{Cu}_2\text{O}$  grains. The average thickness of the  $\text{Cu}_2\text{O}$  layer was estimated to be approximately  $0.68 \mu\text{m}$  from the cross-sectional image, although the thickness varied largely depending on the location.

Angular  $\text{Cu}_2\text{O}$  grains were densely deposited without any vacancy over the entire surface for deposition potentials of  $-0.4$  and  $-0.5 \text{ V}$ , and no underlying  $\text{CuO}$  was observed to be exposed to the surface. The pristine  $\text{Cu}_2\text{O}$  grains stacked over the thorn-like  $\text{CuO}$  grains with excellent adhesivity, and defects



**Figure 3.** Surface (A) and cross-sectional images (B) for  $\text{Cu}_2\text{O}/\text{CuO}$  bi-layers prepared at  $-0.3$  (a),  $-0.4$  (b),  $-0.5$  (c),  $-0.7$  (d), and  $-1.0$  V (e) for the photoelectrochemical  $\text{Cu}_2\text{O}$  deposition.



**Figure 4.** EQE for  $\text{Cu}_2\text{O}/\text{CuO}$  bi-layers prepared at  $-0.3$  (a),  $-0.4$  (b),  $-0.5$  (c), and  $-0.7$  (d) for the photoelectrochemical  $\text{Cu}_2\text{O}$  deposition without (black ●) and with bias voltage of  $-0.02$  (yellow ●),  $-0.04$  (green ●),  $-0.06$  (blue ●),  $-0.08$  (violet ●), and  $-0.1$  V (red ●).

such as pores and vacancies could not be located throughout the entire  $\text{Cu}_2\text{O}/\text{CuO}$  bilayers: neither in the single layers of  $\text{Cu}_2\text{O}$  and  $\text{CuO}$  nor at the heterointerfaces of  $\text{Cu}_2\text{O}/\text{CuO}$  and  $\text{CuO}/\text{FTO}$ -substrates. Both the grain size and thickness for the  $\text{Cu}_2\text{O}$  layers increased to  $550$  nm and  $0.96$   $\mu\text{m}$  with the shift in potential from  $-0.3$  to  $-0.4$  V but decreased to  $416$  nm and  $0.72$   $\mu\text{m}$  at  $-0.5$  V, as observed from the cross-sectional images.

At  $-0.7$  V, angular  $\text{Cu}_2\text{O}$  grains with an average decreased size of approximately  $280$  nm were deposited at a low density on the  $\text{CuO}$  layer, and thorn-like  $\text{CuO}$  grains were observed exposed in spaces between the isolated  $\text{Cu}_2\text{O}$  grains. The thorn-like  $\text{CuO}$  grains were similarly observed uncovered at the surface at  $-1.0$  V, in addition to more sparsely populated  $\text{Cu}_2\text{O}$  grains with  $230$ – $690$  nm in size. The  $\text{Cu}_2\text{O}$  grain size was slightly smaller than that for the  $\text{Cu}_2\text{O}$  layer prepared by electrodeposition<sup>24</sup> and larger than that prepared by thermal oxidation of a  $\text{Cu}$  sheet.<sup>36</sup> While metallic  $\text{Cu}$  species could be detected by the X-ray diffraction measurement, it was difficult to distinguish the  $\text{Cu}$  grains from  $\text{Cu}_2\text{O}$  from the FE-SEM images. Moreover, because the thorn-like  $\text{CuO}$  grain morphology remained unscathed after the  $\text{Cu}_2\text{O}$  deposition at  $-0.7$  and  $-1.0$  V, it is evident that the reduction reaction for

the  $\text{Cu}_2\text{O}$  and  $\text{Cu}$  electrodeposition do not affect the  $\text{CuO}$  grain structure.

The  $\text{Cu}_2\text{O}$  layers prepared at  $-0.7$  and  $-1.0$  V showed increased fwhm values of over  $0.40^\circ$ , compared to  $0.23^\circ$  at potentials ranging from  $-0.3$  to  $-0.5$  V. The fwhm value ( $\beta$ ) of a diffracted X-ray peaks is mainly composed of the instrumental broadening ( $\beta_i$ ), grain size ( $\tau$ ) broadening ( $\beta_\tau$ ), and heterogenous strain ( $\epsilon$ ) broadening ( $\beta_\epsilon$ ), which is shown as follows<sup>37</sup>

$$\beta^2 = \beta_i^2 + \beta_\tau^2 + \beta_\epsilon^2$$

while  $\beta_\tau = \frac{K\lambda}{\tau \cos \theta}$  (Scherrer equation), where  $K$ ,  $\lambda$ ,  $\tau$ , and  $\theta$ , respectively, represents the shape constant at a value of  $0.9$ , wavelength of X-ray, mean crystal dimension, and the Bragg angle. Also,  $\beta_\epsilon = 4\epsilon \tan \theta$ , where  $\epsilon$  represents the heterogenous strain.<sup>38</sup>

The grain size broadening ( $\beta_\tau$ ) was estimated to be  $0.018$ – $0.036^\circ$  from the  $\text{Cu}_2\text{O}$  grain size using the abovementioned Scherrer equation, and the effect of the grain size broadening was limited to the change in fwhm values. The increase in fwhm values originated mainly from the increase in

heterogeneous strain incorporated into the Cu<sub>2</sub>O layer when deposited at potentials below -0.7 V.

The absorption spectra for Cu<sub>2</sub>O/CuO prepared from -0.3 to -1.0 V depositions of Cu<sub>2</sub>O and the relationship of absorption coefficient ( $\alpha$ ) to photon energy ( $h\nu$ ) for the Cu<sub>2</sub>O/CuO bilayers prepared at -0.4 V are shown in Figure S2. The absorption coefficient ( $\alpha$ ) was calculated from the absorbance and total thickness estimated from the cross-sectional images. Two absorption edges could be observed clearly at approximately 580 and 820 nm for all the Cu<sub>2</sub>O/CuO bilayers. The relationship between the band gap energy ( $E_g$ ), absorption coefficient ( $\alpha$ ), and photon energy ( $h\nu$ ) for a direct- and indirect-transition semiconductors is as follows

$$(\alpha h\nu)^n \propto (h\nu - E_g),$$

where  $n = 2$ , and  $1/2$  for direct- and indirect  
-transitions

The p-Cu<sub>2</sub>O and p-CuO semiconductors prepared by electrodeposition were reported to be direct- and indirect-transition type semiconductors.<sup>24,25</sup> The band gap energies estimated by extrapolating the linear part to  $(\alpha h\nu)^n = 0$  were 2.1 and 1.5 eV for Cu<sub>2</sub>O and CuO, respectively, irrespective of the potentials, which agreed with those already reported.

Figure 4 shows the EQE curves for Cu<sub>2</sub>O/CuO bilayers prepared from -0.3 to -0.7 V for the Cu<sub>2</sub>O deposition with and without bias voltages ranging from -0.02 to -0.1 V. The Cu<sub>2</sub>O/CuO bilayer prepared at -0.3 V showed no photovoltaic feature with large fluctuations on the EQE curve at wavelengths ranging from 350 to 950 nm, and the bias voltage possessed no influence on the EQE curve.

Smooth EQE curves with suppressed fluctuations were obtained for the Cu<sub>2</sub>O/CuO bilayer prepared at -0.4 V. The Cu<sub>2</sub>O/CuO bilayer showed a peak of 0.56% in EQE at the wavelength of 510 nm without bias voltage, which increased to a maximum value of 56.8% with the increase in bias voltage to -0.1 V. The photovoltaic feature disappeared when a bias voltage over -0.12 V was applied. The EQE curve recorded at -0.1 V bias voltage increased gradually with the decrease in wavelength from approximately 900 to 670 nm, which rapidly increased to the maximum value at 510 nm. The EQE value then decreased to 36% with the decrease in wavelength at 410 nm, with a shoulder appearing at shorter wavelengths after the peak.

The Cu<sub>2</sub>O/CuO bilayer prepared at -0.5 V showed no photovoltaic feature over the wavelength range of 350 to 950 nm without bias voltages but showed a photovoltaic feature when a bias voltage of -0.1 V was applied, with the maximum EQE value of 1.2% at 580 nm in wavelength. Moreover, the EQE values were estimated to be almost zero at wavelengths shorter than 410 nm. For Cu<sub>2</sub>O/CuO bilayers prepared at -0.7 and -1.0 V, no photovoltaic features were observed along the measured wavelength range, irrespective of the bias voltage. In short, only the Cu<sub>2</sub>O/CuO bilayers prepared at -0.4 and -0.5 V revealed EQE characteristics under bias voltages, but the maximum EQE values were starkly different, and no photovoltaic feature could be observed for the Cu<sub>2</sub>O/CuO bilayers prepared at -0.3, -0.7, and -1.0 V.

As comparison, a single Cu<sub>2</sub>O layer prepared with a similar method but without light irradiation possessed photovoltaic feature at wavelengths ranging from 640 nm roughly corresponding to the band gap energy to 350 nm without

bias voltage, and the maximum EQE value reached 79.7% at 390 nm. The maximum EQE value was enhanced to 99.9% at 410 nm by heating at 423 K under vacuum. With decrease in wavelength from 640 to 510 nm, the EQE value increased slightly from zero to 19%, which then rapidly increased to the maximum value along with the decrease in wavelength for the electrodeposited and heated Cu<sub>2</sub>O layer.<sup>29</sup>

On the other hand, photovoltaic feature was also reported at wavelengths shorter than 900 nm for a single CuO layer prepared by chemical bath deposition followed by heating in air, and the maximum EQE value with external biasing was reported to be approximately 43% at 525 nm in wavelength.<sup>30</sup> The EQE value increased from zero to the maximum value with decrease in wavelength from approximately 900 to 525 nm and then decreased linearly with wavelength.

A 20 nm thick CuO/1.9  $\mu$ m thick Cu<sub>2</sub>O bilayer prepared by the Cu<sub>2</sub>O electrodeposition and followed by heating in air showed a photovoltaic feature at wavelengths from approximately 900 to 300 nm, and a maximum EQE value of 18% was reported at 370 nm under bias voltage.<sup>17</sup> Moreover, the EQE curve with two peaks at 415 and 552 nm in wavelengths was reported for CuO/Cu<sub>2</sub>O bilayers prepared in the same manner but under a different heating condition.<sup>37</sup> The profile and maximum value of the EQE curve varied depending on the preparation condition, which affected the thickness and quality for both the Cu<sub>2</sub>O and CuO layers. Both the Cu<sub>2</sub>O and CuO layers acted as the photovoltaic layer in the Cu<sub>2</sub>O/CuO bilayer, and the resultant EQE curve was a convolution of photovoltaic features originating from both the Cu<sub>2</sub>O and CuO layers.

In this research study, the Cu<sub>2</sub>O/CuO bilayer prepared at -0.4 V revealed a photovoltaic feature at wavelengths from approximately 900 to 350 nm, and the profile of the EQE curve was slightly different to that already reported for the single CuO layer, such as shown in the presence of a shoulder at wavelengths shorter than 510 nm. This indicates that the shoulder originated from the photovoltaic feature of the Cu<sub>2</sub>O layer, and both the Cu<sub>2</sub>O and CuO act as photovoltaic layers in the Cu<sub>2</sub>O/CuO bilayer. On the other hand, the Cu<sub>2</sub>O/CuO bilayer prepared at -0.3 and -0.5 V showed either no or poor photovoltaic feature at a 1.2% maximum EQE value at 580 nm, which shifted from that of -0.4 V at 510 nm.

The optical absorption spectra were almost the same in profile and absorbance for the Cu<sub>2</sub>O/CuO bilayers prepared from -0.3 to -0.5 V as shown in Figure S2, and the optical absorption coefficients were almost constant with a similar total thickness of around 2  $\mu$ m. Thus, the difference in optical absorption characteristic among the Cu<sub>2</sub>O/CuO bilayers prepared from -0.3 to -0.5 V had a limited effect on their photovoltaic behavior.

As observed from the FE-SEM images, there were differences in coverage and grain size for the Cu<sub>2</sub>O layers among the Cu<sub>2</sub>O/CuO bilayers fabricated from -0.3 to -1.0 V. The continuous Cu<sub>2</sub>O layer with a slightly large grain size covered the entire CuO layer at -0.4 V, but exposed CuO surface was observed due to poor coverage of the Cu<sub>2</sub>O layer at -0.3 V. Moreover, for -0.5 V, the Cu<sub>2</sub>O layer possessed excellent coverage, but the grain size decreased. Furthermore, the application of bias voltage was a dominant factor in affecting the EQE characteristics for the Cu<sub>2</sub>O/CuO bilayer prepared at -0.4 and -0.5 V, although there were no effects for those prepared at -0.3, -0.7, and -1.0 V. The bias voltage and grain structures of the Cu<sub>2</sub>O layer could have affected the

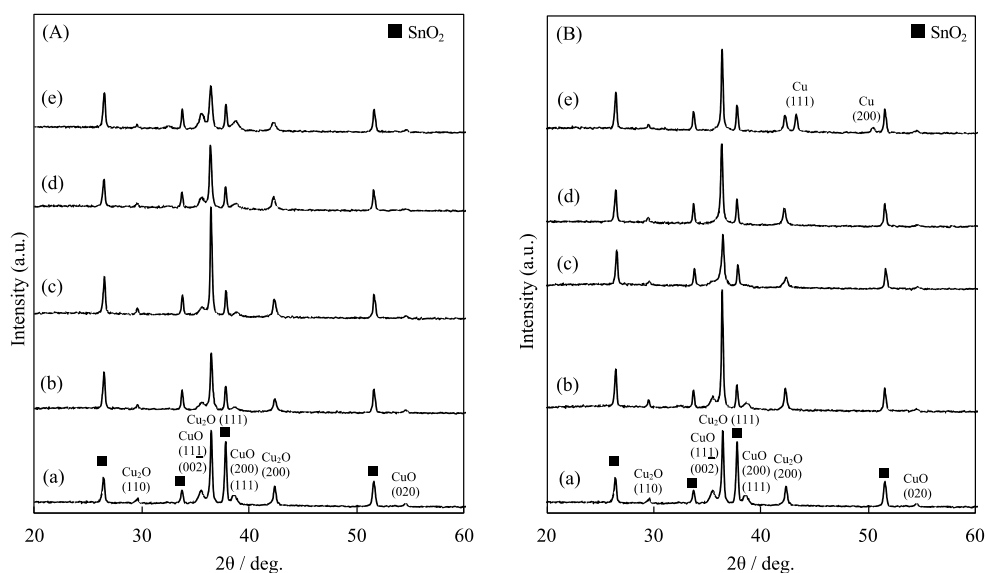


**Figure 5.** X-ray diffraction patterns for Cu<sub>2</sub>O/CuO bi-layers prepared at  $-0.4$  V before (a), and after heating at 423 (b), 473 (c), 523 (d), and 573 K (e) in ambient atmosphere (A) and in vacuum (B).

transportation behavior of electrons through the Cu<sub>2</sub>O/CuO bilayer. The relation of the EQE value and short circuit current density ( $J_s$ ) at a certain wavelength ( $\lambda$ ) is represented by the following equation, where  $E_\lambda$  is the photon energy of the irradiated light

$$\text{EQE}(\lambda) = \frac{1240}{\lambda} \cdot \frac{J_s}{E_\lambda} \cdot 100(\%)$$

The short-circuit current densities ( $J_{sc}$ ) estimated under AM1.5 (1 sun) were reported to be  $0.067 \mu\text{A cm}^{-2}$  and  $7.09 \text{ mA cm}^{-2}$  for the photovoltaic devices of electrodeposited CuO<sup>13</sup> and Cu<sub>2</sub>O layers,<sup>39</sup> respectively. Moreover, a high EQE value was reported for the photovoltaic device of the electrodeposited Cu<sub>2</sub>O layer without bias voltage.<sup>29</sup> The short-circuit current density ( $J_{sc}$ ) is reflected by the diffusivity ( $D$ ) and diffusion length ( $L_c$ ), as represented by the following equation<sup>15,40</sup>

$$D = \frac{kT}{q} \mu_c, \quad L_c = \sqrt{D \cdot \tau_c}$$

where  $q$ ,  $K$ ,  $T$ ,  $\mu_c$ , and  $\tau_c$  are the charge of electron, the Boltzmann constant, temperature, carrier mobility, and life time, respectively.

The electrodeposited Cu<sub>2</sub>O layer possessed a carrier mobility of  $1.8 \text{ cm}^2 \text{ V}^{-1} \text{ s}^{-1}$  for a randomly oriented layer,<sup>24</sup> and  $4\text{--}21 \text{ cm}^2 \text{ V}^{-1} \text{ s}^{-1}$  for a (111)-out-of-plane-oriented layer as measured by the Hall measurement.<sup>41,42</sup> The mobility of an electrodeposited CuO layer is not clear, but the resistivity was reported to be exceptionally high in the order of  $10^5 \Omega \text{ cm}$ .<sup>43</sup> Also, a low carrier mobility in the order of  $10^{-2} \text{ cm}^2 \text{ V}^{-1} \text{ s}^{-1}$  was reported for a single crystal CuO with Hall measurement.<sup>44</sup> Based on these results, it can be deduced that the diffusion length of the carriers could be very short for the CuO layer, compared to that for the electrodeposited Cu<sub>2</sub>O layer. Under light irradiation, electrons were excited in the Cu<sub>2</sub>O layer and swept down to the CuO layer. At the same time, electrons were also excited in the CuO layer, but the probability of these electrons reaching the electrode was low due to the short diffusion length inside the CuO layer. This

contributes to the reason for the very low EQE value for the Cu<sub>2</sub>O/CuO bilayer without bias voltage. The applied bias voltage induced strengthening of the electric fields applied to the carriers inside the CuO layer and near the heterointerface between the Cu<sub>2</sub>O and CuO layers, resulting in the increase in photocurrent density.<sup>40</sup> It is speculated that a continuous Cu<sub>2</sub>O layer is needed to homogeneously apply the electric field toward the CuO layer. Thus, application of bias voltage and having a continuous layered structure were prerequisites to realize an excellent photovoltaic performance for the Cu<sub>2</sub>O/CuO bilayer, which was reflected in a high EQE value, as observed in Figure 4b.

**Heated Cu<sub>2</sub>O/CuO Bilayers and the Photovoltaic Characteristics.** Figure 5 shows the X-ray diffraction patterns for the Cu<sub>2</sub>O/CuO bilayers before and after heating from 423 to 573 K in an ambient atmosphere and vacuum. The diffracted X-ray peaks identified as CuO and Cu<sub>2</sub>O layers were observed for almost all the Cu<sub>2</sub>O/CuO bilayers, and the peak angles showed insignificant changes for both the Cu<sub>2</sub>O and CuO layers, irrespective of the heating temperature and atmosphere. Also, the intensity ratios of peaks for Cu<sub>2</sub>O (110), (111), and (200), and those for CuO (002), (111), and (020) were almost constant, indicating that there were no significant changes in the preferred orientation for both the Cu<sub>2</sub>O and CuO layers.

For heating in an ambient atmosphere, the intensity of the CuO (002) peak increased, while the intensity of the Cu<sub>2</sub>O (111) peak decreased over 523 K, suggesting the occurrence of thermal oxidation from Cu<sub>2</sub>O to CuO phase because CuO is a stable phase under that heating condition.<sup>45</sup> The Cu<sub>2</sub>O (111) peak possessed a minimum fwhm value of approximately  $0.20^\circ$  at 423 K, and the value increased to  $0.32^\circ$  with the rise in heating temperature to 573 K, as shown in Figure S3. The fwhm value of the CuO (002) peak slightly increased from  $0.57$  to  $0.60^\circ$  by 473 K heating, which then decreased to  $0.50^\circ$  with the further rise in heating temperature to 573 K. All the Cu<sub>2</sub>O/CuO bilayers possessed two optical absorption edges at approximately 585 and 820 nm originating from the Cu<sub>2</sub>O and CuO layers, as shown in Figure S4. The Cu<sub>2</sub>O absorption edge at 585 nm slightly became indistinct at heating temperatures

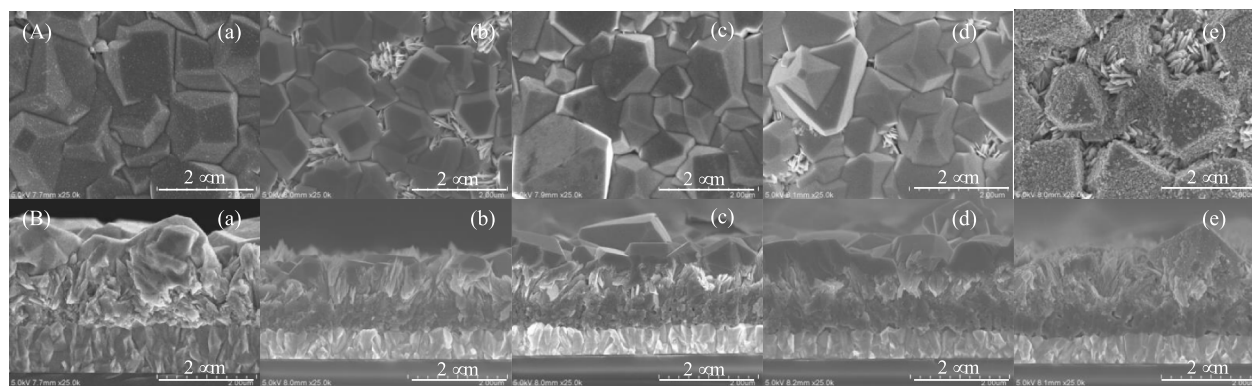


**Figure 6.** Surface (A) and cross-sectional images (B) for  $\text{Cu}_2\text{O}/\text{CuO}$  bi-layers prepared at  $-0.4$  V before (a), and after heating at 423 (b), 473 (c), 523 (d), and 573 K (e) in ambient atmosphere.

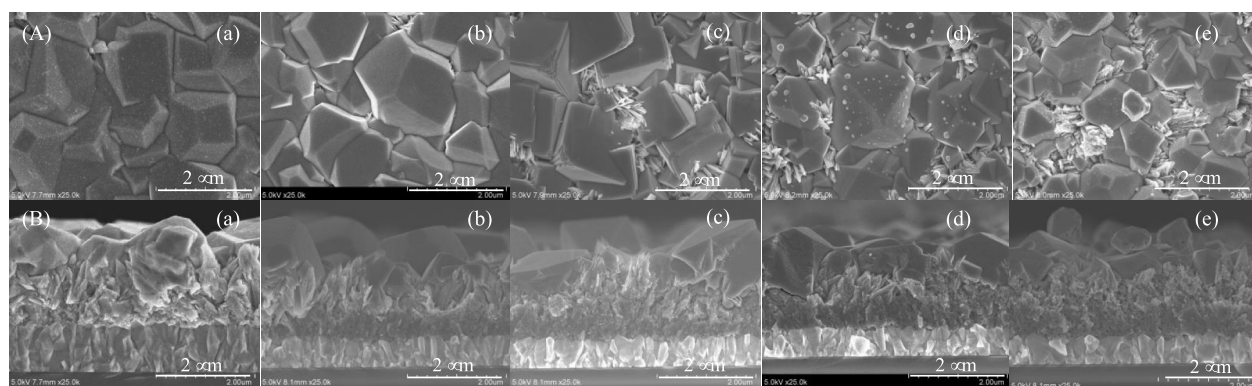


**Figure 7.** Surface (A) and cross-sectional images (B) for  $\text{Cu}_2\text{O}/\text{CuO}$  bi-layers prepared at  $-0.4$  V before (a), and after heating at 423 (b), 473 (c), 523 (d), and 573 K (e) in vacuum.

over 523 K, and the change was consistent with the decrease in intensity of the  $\text{Cu}_2\text{O}$  (111) peak.

Similarly, the diffracted X-ray peaks identified as  $\text{Cu}_2\text{O}$  and  $\text{CuO}$  layers could be observed clearly at heating temperature below 473 K in vacuum. However, the  $\text{CuO}$  peaks disappeared when heated at temperatures over 523 K, and peaks originating from metallic  $\text{Cu}$  appeared at the 573 K. Heating in vacuum induced both the reduction reactions from  $\text{CuO}$  to  $\text{Cu}_2\text{O}$ , and from  $\text{Cu}_2\text{O}$  to  $\text{Cu}$ . The fwhm values of the  $\text{Cu}_2\text{O}$  (111) peak decreased to the minimum value of  $0.22^\circ$  by the 423 K heating, which then increased to  $0.23^\circ$  with the rise in heating temperature to 573 K, as shown in Figure S3. The fwhm values of the  $\text{CuO}$  (002) peak showed an almost constant value around  $0.57^\circ$  before and after heating at 423 K, which increased to  $0.60^\circ$  when heated at 473 K. The absorption edges at 585 and 821 nm were observed for the  $\text{Cu}_2\text{O}/\text{CuO}$  bilayers heated below 473 K, but the  $\text{CuO}$  absorption edge became less clear at heating temperatures higher than 523 K, as shown in Figure S4. Also, absorbance over 585 nm in wavelength increased after heating at 573 K, and the increase was attributed to the formation of opaque metallic  $\text{Cu}$  by thermal reduction reaction.

Figure 6 shows the surface and cross-sectional images for the  $\text{Cu}_2\text{O}/\text{CuO}$  bilayers before and after heating at temperatures from 423 to 573 K in an ambient atmosphere. The  $\text{Cu}_2\text{O}/\text{CuO}$  bilayers before and after heating at 423 K were almost identical in both the surface and cross-sectional structures, and the  $\text{Cu}_2\text{O}$  grains with an average size of approximately 550 nm formed a relatively smooth and continuous surface. The  $\text{Cu}_2\text{O}$  layers were grown adhering to the thorn-like  $\text{CuO}$  grains, and

defects such as vacancy or voids could be located neither throughout the  $\text{Cu}_2\text{O}/\text{CuO}$  bilayers nor near the heterointerface.

The surface morphology of the  $\text{Cu}_2\text{O}/\text{CuO}$  bilayers heated at 473 and 523 K were similar to that for 423 K, and the  $\text{Cu}_2\text{O}$  grain size remained at approximately 550 nm. An irregularity, however, was observed on the  $\text{Cu}_2\text{O}$  surface after the 523 K heating, which showed granular grains with 20–30 nm in size forming over the entire  $\text{Cu}_2\text{O}$  surface after heating at 573 K. From the diffracted X-ray, the decrease in  $\text{Cu}_2\text{O}$  peak intensity but an increase in  $\text{CuO}$  peak intensity indicate that the small granular grains were  $\text{CuO}$  grains. In addition, the thorn-like  $\text{CuO}$  grains in the surface image of 573 K appeared to be grown from the bottom layer.

The changes in the grain structure were generally induced when the  $\text{CuO}$  layers were heated above 473 K, and the resultant layer was composed of thorn-like grains on the top layer and granular grains at the bottom, although these actual grain sizes could not be ascertained from the cross-sectional images. Additionally, the formation of nanopores with 20–30 nm in sizes inside the granules of the bottom  $\text{CuO}$  layer and near its heterointerface to the FTO substrate could be discerned. These pore sizes were observed to increase with the rise in heating temperature, and eventually spatial gaps of 200–300 nm in lengths and approximately 100 nm in widths were formed near the  $\text{CuO}/\text{FTO}$  heterointerfaces after heating at 523 K.

The fwhm value of the  $\text{Cu}_2\text{O}$  (111) peaks decreased from  $0.26^\circ$  to a minimum value of  $0.22^\circ$  by heating at 423 K, which then increased to  $0.32^\circ$  with the rise in heating temperature to

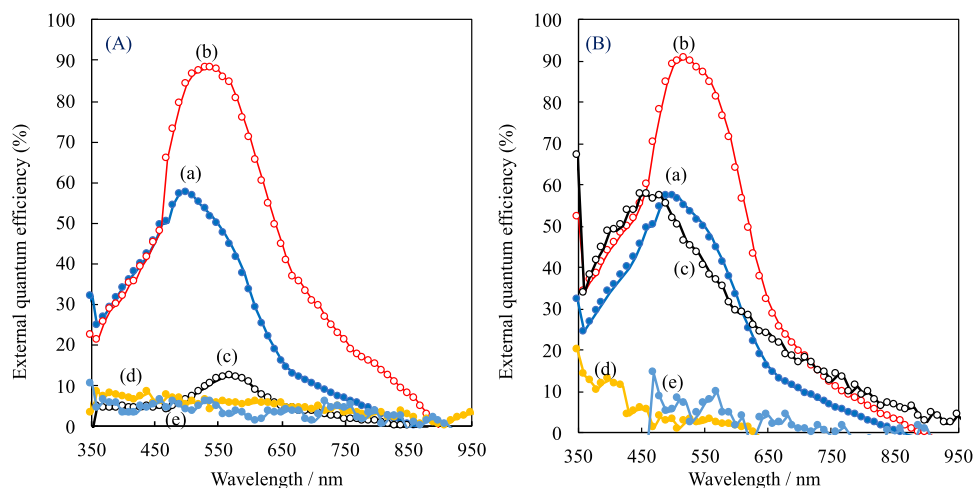


**Figure 8.** EQE for  $\text{Cu}_2\text{O}/\text{CuO}$  bi-layers prepared at  $-0.4$  V (a), and heated at 423 (b), 473 (c), 523 (d), and 573 K (e) in ambient atmosphere (A) and vacuum (B) with the bias voltage of  $-0.1$  V.

573 K. Because the  $\text{Cu}_2\text{O}$  grain sizes were almost constant irrespective of the heating temperature, the change in the fwhm value could be deduced originated from the heterogenous strain, indicating that strain relaxation in the  $\text{Cu}_2\text{O}$  layer was optimum when heated at 423 K, which yielded a minimum strain. The almost constant fwhm values for the CuO layers before and after heating at 423 K was consistent to the fact that they possessed virtually identical grain structures, and the fwhm value decreased from 473 K, at which the CuO grain structure began to change. Because the grain sizes could not be estimated from the FE-SEM image for the CuO layers, by the heating over 473 K, it induced either a decrease in heterogenous strain or an increase in the grain size.

Figure 7 shows the surface and cross-sectional images for the  $\text{Cu}_2\text{O}/\text{CuO}$  bilayers before and after heating at temperatures from 423 to 573 K in vacuum. The  $\text{Cu}_2\text{O}$  layer exhibited angular grains with approximately 550 nm in size and a smooth surface and entirely covered the CuO layer before and after heating at 423 K. The CuO layer retained the thorn-like grain structure adhering to the upper  $\text{Cu}_2\text{O}$  layer without any defects such as pores or voids observed in the  $\text{Cu}_2\text{O}/\text{CuO}$  bilayer. The  $\text{Cu}_2\text{O}$  grain size showed an almost constant value at approximately 550 nm even when heated above 473 K, but small grains begin to emerge on the  $\text{Cu}_2\text{O}$  surface when heated above 523 K, and thorn-like CuO grains started to appear clearly at the spaces between the  $\text{Cu}_2\text{O}$  grains as seen from the surface image.

The change in morphology from the thorn-like grains to granular grains for the bottom CuO layer was observed after heating above 473 K, but the upper CuO layer retained its thorn-like grain morphology. Furthermore, the formation of nanopores was confirmed inside the granules of the bottom CuO. The 523 K heating induced the coalescence of nanopores inside the granular CuO bottom layer and led to the eventual formation of spatial gaps near the heterointerfaces to both the  $\text{Cu}_2\text{O}$  layer and FTO substrate, similar to that of layers annealed in ambient atmosphere at the same temperatures.

The fwhm value for the  $\text{Cu}_2\text{O}$  layer decreased to a minimum value of  $0.22^\circ$  after heating at 423 K, which then slightly increased with the rise in heating temperature. The  $\text{Cu}_2\text{O}$  grain size possessed a constant value irrespective of the heating temperature, indicating that the  $\text{Cu}_2\text{O}$  layer heated at 423 K

was at a state of minimum strain. The fwhm value for the CuO layer also increased by heating at 473 K, at which the CuO grain structure began to change.

Figure 8 shows the EQE curves for  $\text{Cu}_2\text{O}/\text{CuO}$  bilayers prepared at  $-0.4$  V and heated at temperatures from 423 to 573 K in an ambient atmosphere and vacuum with a bias voltage of  $-0.1$  V. The  $\text{Cu}_2\text{O}/\text{CuO}$  bilayers prepared at  $-0.4$  V revealed its photovoltaic feature at wavelengths ranging from 350 nm to approximately 900 nm, and a maximum EQE value of 56.8% was obtained at 510 nm. The 423 K heating in an ambient atmosphere brought the enhancement of the EQE value at wavelengths ranging from 460 to 900 nm, and the maximum EQE value increased to 87.7% at 550 nm. The EQE curve after heating at 423 K showed a similar profile to that before heating, at wavelengths below 460 nm. The EQE curve for the  $\text{Cu}_2\text{O}/\text{CuO}$  bilayers was a convolution of the EQE profiles of the  $\text{Cu}_2\text{O}$  and CuO layers, where EQE peaks were reported to be located at around 410 and 520 nm for single  $\text{Cu}_2\text{O}$  and CuO layers.<sup>28,29</sup> According to these results, the enhancement of the EQE values at wavelengths from 460 to 900 nm was attributed to the improvement of the photovoltaic performance of the CuO layer. The 473 K heating, however, resulted in a reduction of EQE values over the whole wavelength range recorded, and the maximum EQE value decreased to 11.6% at 550 nm. The EQE value at wavelengths below 460 nm decreased to almost zero, indicating that the photovoltaic feature for the  $\text{Cu}_2\text{O}$  layer had disappeared. The  $\text{Cu}_2\text{O}/\text{CuO}$  bilayers heated at elevated temperatures above 523 K showed no photovoltaic feature irrespective of the wavelength.

The 423 K heating in vacuum brought enhancement of photovoltaic performance over the wavelengths ranging from 350 nm to approximately 900 nm, and the maximum EQE value increased to 89.8% at 530 nm in wavelength. The increase in the EQE value was estimated to be 12.6% and 33.0% at wavelengths of 410 and 520 nm, at which the single  $\text{Cu}_2\text{O}$  and CuO layered showed their maximum EQE values. Because the EQE curve for the  $\text{Cu}_2\text{O}/\text{CuO}$  bilayer was a convolution of the EQE for both the  $\text{Cu}_2\text{O}$  and CuO layers as mentioned above, the enhancement of the performance could be attributed to the overall improvements of the photovoltaic performance for both the  $\text{Cu}_2\text{O}$  and CuO layers. The EQE curve after heating at 473 K was almost similar in profile and

EQE value at wavelengths shorter than 460 nm to that heated at 423 K, but the EQE values at wavelengths above 460 nm declined drastically. The maximum EQE value was reduced to 57.5%, accompanied by a shift in the peak wavelength to 460 nm, suggesting a drastic deterioration in the photovoltaic performance of the CuO layer when heated at 473 K. The Cu<sub>2</sub>O/CuO bilayer heated above 523 K showed no photovoltaic feature irrespective of the wavelength, and the photovoltaic performance had disappeared for both the Cu<sub>2</sub>O and CuO layers.

In short, the photovoltaic performance was enhanced by heating at 423 K for the Cu<sub>2</sub>O/CuO bilayers, and a high EQE value around 90% was achieved in both ambient atmosphere and vacuum. Because the light absorption characteristics were almost identical in profile and absorbance for the Cu<sub>2</sub>O/CuO bilayers before and after heating at 423 K in both atmospheres, the enhancement of the EQE values could have originated from the improvements of carrier transportation, and not in light absorption. The Cu<sub>2</sub>O layers heated at 423 K were at states of minimum strain, as evidenced from the decreases in the fwhm values of the diffracted X-ray peaks in both atmospheres. Because the carrier transportation process generally reflects the existence of defects such as lattice defects and impurities, this also means that the minimization of heterogenous strain from lessening the lattice defects and impurities, which act as scattering defects suppressing the carrier transportation, was achieved. For the CuO layer, effects of the 423 K heating on the fwhm value showed a different dependence on the atmosphere. The 423 K heating in vacuum induced either the decrease in heterogenous strain or increase in the grain size from the decrease in the fwhm value, but both have favorable effects on the carrier transportation. On the other hand, the increase in the fwhm value was brought about by heating in 423 K in an ambient atmosphere, but the resistivity of the CuO layer prepared in this manner was reported to decrease when heated in ambient atmosphere.<sup>43</sup> The resistivity ( $\rho$ ) for p-type semiconductors is a function of the carrier concentration ( $n$ ) and mobility ( $\mu$ ) as follows

$$1/\rho = e \cdot n \cdot \mu$$

where  $e$  is the electric charge of electron. The enhancement of photovoltaic performance by heating at 423 K was attributed to the amelioration of the electrical characteristics including carrier mobility for both the Cu<sub>2</sub>O and CuO layers. Further investigations on the Hall effect measurements are needed to clarify the improvement of the carrier mobility, although there was a difficulty on the layer isolation due to high adhesion.<sup>24</sup>

The photovoltaic feature for the Cu<sub>2</sub>O/CuO bilayers deteriorated and disappeared by heating at 473 K and above 523 K in both atmospheres. The harmful effects of nanopores and related defects on the photovoltaic performances for both the Cu<sub>2</sub>O and CuO layers have been demonstrated for the CuO/Cu<sub>2</sub>O bilayers prepared by the Cu<sub>2</sub>O electrodeposition followed by heating in ambient atmosphere.<sup>17</sup> The change in grain structure of the CuO layer and the formation of nanopores were confirmed from the structural analysis by FE-SEM observation, which was the principal reason for the deterioration and disappearance of the photovoltaic feature for the Cu<sub>2</sub>O/CuO bilayers when heated above 473 K.

## CONCLUSIONS

The Cu<sub>2</sub>O/CuO bilayers were prepared by electrodeposition of the CuO layer in a copper(II)–ammonia complex aqueous

solution, followed by the photoelectrochemical deposition of the Cu<sub>2</sub>O layer in a copper(II)–lactate complex aqueous solution under light irradiation. The CuO layers possessed a characteristic band gap energy of 1.5 eV and were composed of thorn-like grains, while the Cu<sub>2</sub>O layers with a characteristic 2.1 eV band gap energy adhesively stacked on the CuO layer at potentials of  $-0.4$  to  $-0.5$  V referenced to an Ag/AgCl electrode when photoelectrochemical deposited, and additional metallic Cu were co-deposited at potentials more negative than  $-0.7$  V. Dense and defect-free Cu<sub>2</sub>O/CuO bilayers could be successfully fabricated at potentials of  $-0.4$  and  $-0.5$  V, with decreased Cu<sub>2</sub>O grain sizes at  $-0.5$  V.

The Cu<sub>2</sub>O/CuO bilayers prepared at  $-0.4$  V revealed photovoltaic features at wavelengths ranging from 350 nm to approximately 900 nm with the maximum EQE value of 56.8% at 510 nm under an applied bias voltage of  $-0.1$  V, and both the Cu<sub>2</sub>O and CuO layers acted as the photovoltaic layers in this bilayer. The maximum EQE value, however, drastically decreased to 1.2% accompanying the shift of the peak wavelength to 580 nm, and no photovoltaic features could be observed for Cu<sub>2</sub>O/CuO bilayers prepared at  $-0.3$ ,  $-0.7$ , and  $-1.0$  V.

The photovoltaic performance for the Cu<sub>2</sub>O/CuO bilayer fabricated at  $-0.4$  V was enhanced by heating at 423 K, and the maximum EQE value increased to 87.7% and 89.8% in ambient atmosphere and vacuum, respectively. The electrical characteristics including the carrier mobility for both the Cu<sub>2</sub>O and CuO layers strongly affected the photovoltaic performances of the Cu<sub>2</sub>O/CuO bilayers. The photovoltaic feature, however, disappeared when heated above 523 K, due to the formation of nanopores inside the CuO layers and spatial gaps near the CuO heterointerfaces to the Cu<sub>2</sub>O layer and FTO substrate.

The results demonstrated here revealed the possibility and feasibility of the Cu<sub>2</sub>O/CuO bilayer prepared by electrochemical reaction and heating as a photovoltaic layer applicable to solar cells and photocathode for photoelectrochemical water splitting.

## ASSOCIATED CONTENT

### Supporting Information

The Supporting Information is available free of charge at <https://pubs.acs.org/doi/10.1021/acsomega.1c05163>.

fwhm values before and after heating; absorption spectra for bilayers before and after heating (PDF)

## AUTHOR INFORMATION

### Corresponding Author

Masanobu Izaki – Graduate School of Engineering, Toyohashi University of Technology, Toyohashi-shi, Aichi 441-8580, Japan; [orcid.org/0000-0002-3959-1923](https://orcid.org/0000-0002-3959-1923); Email: [m-izaki@me.tut.ac.jp](mailto:m-izaki@me.tut.ac.jp)

### Authors

Suzuka Abe – Graduate School of Engineering, Toyohashi University of Technology, Toyohashi-shi, Aichi 441-8580, Japan; Present Address: LIXIL Corporation, S-1, Koiehonmachi, Tokoname-city, Aichi, 479-8585, Japan

Kota Nakakita – Graduate School of Engineering, Toyohashi University of Technology, Toyohashi-shi, Aichi 441-8580, Japan

Pei Loon Khoo – Graduate School of Engineering, Toyohashi University of Technology, Toyohashi-shi, Aichi 441-8580, Japan

Complete contact information is available at:  
<https://pubs.acs.org/10.1021/acsoomega.1c05163>

### Author Contributions

M.I. conceived the project, designed the experiments and analyzed data. S.A., K.N., and K.P.L. carried out the material preparation and most of characterizations. All authors discussed the results and commented on the manuscript.

### Notes

The authors declare no competing financial interest.

### ACKNOWLEDGMENTS

This work was supported in part by a Grant-in-Aid for Scientific Research (19H02810).

### REFERENCES

- (1) Yamaguchi, M.; Masuda, T.; Araki, K.; sato, D.; Lee, K.-H.; Kojima, N.; Takamoto, T.; Okumura, K.; Satou, A.; Yamada, K.; Nakado, T.; Zushi, Y.; Yamazaki, M.; Yamada, H. Role of PV-powered vehicles in low-carbon society and some approaches of high-efficiency solar cell modules for cars. *Energy Power Eng.* **2020**, *12*, 375–395.
- (2) Luque, A.; Hegedus, S. *Handbook of Photovoltaic Science and Engineering*; John Wiley & Sons: West Sussex, 2003; pp 70–74.
- (3) Walter, M. G.; Warren, E. L.; Mckone, J. R.; Boettcher, S. W.; Mi, Q.; Santori, E. A.; Lewis, N. S. Solar water splitting cells. *Chem. Rev.* **2010**, *110*, 6446–6473.
- (4) Chopra, K. L.; Paulson, P. D.; Dutta, V. Thin-film solar cells: an overview. *Prog. Photovol.: Res. Appl.* **2004**, *12*, 69–92.
- (5) Sivula, K.; van de Krol, R. Semiconducting materials for photoelectrochemical energy conversion. *Nat. Rev. Mater.* **2016**, *1*, 15010.
- (6) Loferski, J. J. Theoretical considerations governing the choice of the optimum semiconductor for photovoltaic solar energy conversion. *J. Appl. Phys.* **1956**, *27*, 777–784.
- (7) Yamaguchi, M. III-V compound multi-junction solar cells: present and future. *Sol. Energy Mater. Sol. Cells* **2003**, *75*, 261–269.
- (8) Takamoto, T.; Kaneiwa, M.; Imaizumi, M.; Yamaguchi, M. InGaP/GaAs-based multijunction solar cells. *Prog. Photovol.: Res. Appl.* **2005**, *13*, 495–511.
- (9) Koffyberg, F. P.; Benko, F. A. A photoelectrochemical determination of the position of the conduction and valence band edges of p-type CuO. *J. Appl. Phys.* **1982**, *53*, 1173–1177.
- (10) Snoke, D. W.; Shields, A. J.; Cardona, M. Phonon-absorption recombination luminescence of room-temperature excitons in Cu<sub>2</sub>O. *Phys. Rev. B: Condens. Matter Mater. Phys.* **1992**, *45*, 11693–11697.
- (11) Korottcnkov, G. *The Future of Semiconductor Oxides in Next-Generation Solar Cells, All-Oxide Solar Cells*; Elsevier: Cambridge, 2018; pp 439–480.
- (12) Izaki, M.; Shinagawa, T.; Mizuno, K.-T.; Ida, Y.; Inaba, M.; Tasaka, A. Electrochemically constructed p-Cu<sub>2</sub>O/n-ZnO heterojunction diode for photovoltaic devices. *J. Phys. D: Appl. Phys.* **2007**, *40*, 3326–3329.
- (13) Khoo, P. L.; Nagai, M.; Watanabe, M.; Izaki, M. Electrodeposited CuO photovoltaic device with polysiloxane layer. *J. Surf. Finish. Soc. Jpn.* **2018**, *69*, 469–471.
- (14) Li, C.; He, J.; Xiao, Y.; Li, Y.; Delaunay, J.-J. earth-abundant Cu-based metal oxide photocathodes for electrochemical water splitting. *Energy Environ. Sci.* **2020**, *13*, 3269.
- (15) Paracchino, A.; Laporte, V.; Sivula, K.; Grätzel, M.; Thimsen, E. Highly active oxide photocathode for photoelectrochemical water reduction. *Nat. Mater.* **2011**, *10*, 456–461.
- (16) Masudy-Panah, S.; Moakhar, R. S.; Chua, C. S.; Kushwaha, A.; Dalapati, G. K. Stable and efficient CuO based photocathode through oxygen-rich composition and Au-Pd nanostructure incorporation for solar hydrogen production. *ACS Appl. Mater. Interfaces* **2017**, *9*, 27596–27606.
- (17) Izaki, M.; Fukazawa, K.; Sato, K.; Khoo, P. L.; Kobayashi, M.; Takeuchi, A.; Uesugi, K. Defect structure and photovoltaic characteristics of internally stacked CuO/Cu<sub>2</sub>O photoactive layer prepared by electrodeposition and heating. *ACS Appl. Energy Mater.* **2019**, *2*, 4833–4840.
- (18) Yang, Y.; Xu, D.; Wu, Q.; Diao, P. Cu<sub>2</sub>O/CuO bilayered composite as a high-efficiency photocathode for photoelectrochemical hydrogen evolution reaction. *Sci. Rep.* **2016**, *6*, 35158.
- (19) Dubale, A. A.; Ahmed, I. N.; Zhang, Y.-J.; Yang, X.-L.; Xie, M.-H. A facile strategy for fabricating C@Cu<sub>2</sub>O/CuO composite for efficient photochemical hydrogen production with high external quantum efficiency. *Appl. Surf. Sci.* **2020**, *534*, 147582.
- (20) Minami, T.; Nishi, Y.; Miyata, T. Efficiency enhancement using a Zn<sub>1-x</sub>Ge<sub>x</sub>O thin film as an n-type window layer in Cu<sub>2</sub>O-based heterojunction solar cells. *APEX* **2016**, *9*, 052301.
- (21) Wang, P.; Zhao, X.; Li, B. ZnO-coated CuO nanowire arrays: fabrications, optoelectronic properties, and photovoltaic applications. *Opt. Exp.* **2011**, *19*, 11271–11279.
- (22) Paul, G. K.; Nawa, Y.; Sato, H.; Sakurai, T.; Akimoto, K. defects in Cu<sub>2</sub>O studied by deep level transient spectroscopy. *Appl. Phys. Lett.* **2006**, *88*, 141901.
- (23) Bhardwaj, R.; Barman, R.; Kaur, D. Improved photovoltaic effect in CuO/Zn<sub>1-x</sub>Mg<sub>x</sub>O heterojunction solar cell by pulsed laser deposition. *Mater. Lett.* **2016**, *185*, 230–234.
- (24) Mizuno, K.; Izaki, M.; Murase, K.; Shinagawa, T.; Chigane, M.; Inaba, M.; Tasaka, A.; Awakura, Y. Structural and electrical characterizations of electrodeposited p-type semiconductor Cu<sub>2</sub>O films. *J. Electrochem. Soc.* **2005**, *152*, C179–C182.
- (25) Izaki, M.; Nagai, M.; Maeda, K.; Mohamad, F. B.; Motomura, K.; Sasano, J.; Shinagawa, T.; Watase, S. Electrodeposition of 1.4-eV-bandgap-p-copper (II) oxide film with excellent photoactivity. *J. Electrochem. Soc.* **2011**, *158*, D578–D584.
- (26) Zimbovskii, D. S.; Churagulov, B. R. Cu<sub>2</sub>O and CuO films produced by chemical and anodic oxidation on the surface of copper foil. *Inorg. Mater.* **2018**, *54*, 660–666.
- (27) Wijesundera, R. P.; Hidaka, M.; Koga, K.; Choi, J.-Y.; Sung, N. E. Structural and electronic properties of electrodeposited heterojunction of CuO/Cu<sub>2</sub>O. *Ceramics* **2010**, *54*, 19.
- (28) Kim, A.-Y.; Kim, M. K.; Cho, K.; Woo, J.-Y.; Lee, Y.; Han, S.-H.; Byun, D.; Choi, W.; Lee, J. K. One-step catalytic synthesis of CuO/Cu<sub>2</sub>O in a graphitized porous C matrix derived from the Cu-based metal-organic framework for Li- and Na-ion batteries. *ACS Appl. Mater. Interfaces* **2016**, *8*, 19514–19523.
- (29) Khoo, P. L.; Kikkawa, Y.; Satou, K.; Shinagawa, T.; Izaki, M. Improvements in external quantum efficiency of electrochemically constructed n-ZnO/p-Cu<sub>2</sub>O photovoltaic devices by rapid thermal annealing. *Thin Solid Films* **2018**, *653*, 158–164.
- (30) Kaphle, A.; Echeverria, E.; McIlroy, D. N.; Hari, P. Enhancement in the performance of nanostructured CuO-ZnO solar cells by band alignment. *RSC Adv.* **2020**, *10*, 7839–7853.
- (31) Izaki, M.; Koyama, T.; Khoo, P. L.; Shinagawa, T. Light-irradiated electrochemical direct construction of Cu<sub>2</sub>O/CuO bilayers by switching cathodic/anodic polarization in copper(II)-tartrate complex aqueous solution. *ACS Omega* **2020**, *5*, 683–691.
- (32) Chen, T.; Kitada, A.; Seki, Y.; Fukami, K.; Usmanov, D. T.; Chen, L. C.; Hiraoka, K.; Murase, K. Identification of copper(II)-lactate complexes in Cu<sub>2</sub>O electrodeposition baths; Deprotonation of  $\alpha$ -hydroxyl group in highly concentrated alkaline solution. *J. Electrochem. Soc.* **2018**, *165*, D444–D451.
- (33) Chen, T.; Kitada, A.; Fukami, K.; Murase, K.; Murase, K. Determination of stability constants of copper(II)-lactate complexes in Cu<sub>2</sub>O electrodeposition baths by UV-vis absorption spectra factor analysis. *J. Electrochem. Soc.* **2019**, *166*, D761–D767.
- (34) Joint Committee on Powder Diffraction Standards. *Powder Diffraction File*; International Data for Diffraction Data: Swarthmore, PA, 1992; pp 5–667.

- (35) Joint Committee on Powder Diffraction Standards. *Powder Diffraction File*; International Data for Diffraction Data: Swarthmore, PA, 1992; pp 2–1041.
- (36) Minami, T.; Miyata, T.; Nishi, Y. Efficiency improvement of Cu<sub>2</sub>O-based heterojunction solar cells fabricated using thermally oxidized copper sheets. *Thin Solid Films* **2014**, *559*, 105–111.
- (37) Loon Khoo, P.; Satou, K.; Nozaki, K.; Izaki, M. External quantum efficiency of electrochemically prepared and annealed directly stacked SLG/GZO/Cu<sub>2</sub>O/CuO photoactive layer. *J. Phys.: Conf. Ser.* **2018**, *1083*, 012030.
- (38) Jenkins, R.; Snyder, R. L. *Introduction to X-ray Powder Diffractometry*; John Wiley & Sons: New York, 1996; pp 89–94.
- (39) Izaki, M.; Ohta, T.; Kondo, M.; Takahashi, T.; Mohamad, F. B.; Zamzuri, M.; Sasano, J.; Shinagawa, T.; Pauporté, T. Electrodeposited ZnO-nanowire/Cu<sub>2</sub>O photovoltaic device with highly resistive ZnO intermediate layer. *ACS Appl. Mater. Interfaces* **2014**, *6*, 13461–13469.
- (40) Sze, S. M.; Ng, K. K. *Physics of Semiconductor Devices*; John Wiley & Sons: New Jersey, 2007; pp 45–46.
- (41) Izaki, M.; Sasaki, S.; Mohamad, F. B.; Shinagawa, T.; Ohta, T.; Watase, S.; Sasano, J. Effects of preparation temperature on optical and electrical characteristics of (111)-oriented Cu<sub>2</sub>O films electrodeposited on (111)-Au film. *Thin Solid Films* **2012**, *520*, 1779–1783.
- (42) Shinagawa, T.; Onoda, M.; Fariza, B. M.; Sasano, J.; Izaki, M. Annealing effects and photoelectric properties of single-oriented Cu<sub>2</sub>O films electrodeposited on Au(111)/Si(100) substrates. *J. Mater. Chem. A* **2013**, *1*, 9182–9188.
- (43) Izaki, M. Effects of annealing on optical and electrical characteristics of p-type semiconductor copper(II) oxide electrodeposits. *Thin Solid Films* **2012**, *520*, 2434–2437.
- (44) Samokhvalov, A. A.; Viglin, N. A.; Gizhevskii, N. N.; Loshkareva, N. N.; Osipov, V. V.; Solin, N. I.; Sukhorukov, Y. P. Low-mobility charge carriers in CuO. *J. Exp. Theor. Phys.* **1993**, *76*, 463–468.
- (45) Zhu, Y.; Mimura, K.; Isshiki, M. Oxidation mechanism of Cu<sub>2</sub>O to CuO at 600–1050°C. *Oxid. Met.* **2004**, *62*, 207–222.